High Resolution Measurement of Cerebral Blood Flow using Intravascular Tracer Bolus Passages. Part I: Mathematical Approach and Statistical Analysis

Leif Østergaard, Robert M. Weisskoff, David A. Chesler, Carsten Gyldensted, Bruce R. Rosen

The authors review the theoretical basis of determination of cerebral blood flow (CBF) using dynamic measurements of nondiffusible contrast agents, and demonstrate how parametric and nonparametric deconvolution techniques can be modified for the special requirements of CBF determination using dynamic MRI. Using Monte Carlo modeling, the use of simple, analytical residue models is shown to introduce large errors in flow estimates when actual, underlying vascular characteristics are not sufficiently described by the chosen function. The determination of the shape of the residue function on a regional basis is shown to be possible only at high signal-to-noise ratio. Comparison of several nonparametric deconvolution techniques showed that a nonparametric deconvolution technique (singular value decomposition) allows estimation of flow relatively independent of underlying vascular structure and volume even at low signal-to-noise ratio associated with pixel-by-pixel deconvolution.

Key words: cerebral blood flow (CBF); dynamic magnetic resonance imaging (MRI); nonparametric deconvolution; susceptibility contrast.

INTRODUCTION

One of the main goals of functional NMR is noninvasive, high resolution determination of cerebral perfusion. With the development of rapid MR imaging sequences, dynamic imaging of concentration time curves after bolus-injection of purely intravascular contrast agents has become possible on time scales comparable with vascular mean transit times (MTT). Using the central volume theorem (1, 2), these concentration time curves have been used to calculate regional cerebral blood volume (rCBV) using CT (3) and, more recently, MRI (4, 5). Attempts have been made to use bolus passages of intravascular contrast agents to calculate regional CBF (6–8) and myocardial perfusion (9). This technique involves knowledge of vascular structure through the *residue function*, determining how the observed tracer is retained in the vasculature. This has caused some to reject this as a method of determining blood flow since the vascular structure is not known *a priori* (10), whereas others have pursued mathematical and numerical deconvolution approaches to determine both flow and the necessary characteristics of the vascular bed *a posteriori* from measurements (model independent approaches) (7, 8). The latter approach in turn may provide important information about the microvasculature. Other authors have proposed general analytical models to describe the shape of the residue function (model dependent approaches) (11).

In this study we seek to determine a robust mathematical approach to determine flow and vascular tracer retention by deconvolution of dynamic MRI tissue concentration curves with noninvasively determined arterial input curves. We first review the theory and inherent mathematical problems of flow measurements with nondiffusible tracers. Two main categories of nonparametric deconvolution techniques are described and modified for use with MRI determination of rCBF. We then use Monte Carlo simulations to address the possibilities of determining the shape of the vascular residue function using nonparametric deconvolution techniques. Finally, we analyze the errors on the estimated CBF values that may be involved in (i) using simple, analytical expressions to describe the vascular residue function and (ii) using nonparametric deconvolution techniques at signal-to-noise ratios (SNR) typical of dynamic MRI experiments.

THEORY

We briefly review the definitions of the MTT, CBV,and CBF as well as their inter-relationship given by the central volume theorem (1, 2). Given these definitions, we state and discuss the central equation in our approach to the determination of CBF using nondiffusible, paramagnetic MRI tracers.

Consider a bolus of nondiffusible tracer given at time $t = 0$ in the feeding vessel(s) to a volume of interest (VOI) of tissue. The individual particles of the tracer follow different paths through the VOI and their transit times thus have a distribution characteristic of the flow and the vascular structure. The probability density function of these transit times is denoted $h(t)$, the *transport function*. When an arterial input $C_a(t)$ is given to the VOI, the concentration of tracer in the venous output, $C_v(t)$, from

MRM 36:715–725 (1996)

From the MGH-NMR Center, Department of Radiology, Massachusetts General Hospital, Harvard Medical School, Charlestown, Massachusetts; and the Department of Neuroradiology (L.Ø., C.G.) and PET-Center (L.Ø.), Århus University Hospital, Århus, Denmark.

Address correspondence to: Leif Østergaard, M.D., M.S., Department of Neuroradiology, Århus Kommunehospital, Nørrebrogade 44, DK-8000 Århus, Denmark.

Received July 27, 1995; revised January 31, 1996; accepted may 9, 1996.

This work was supported by The Danish Research Academy (S940197), The Danish Medical Research Counsil (12–1634-1, 1993), Danish Physicians' Insurance (under the auspices of Codan Insurance Company, Copenhagen), The Einar Willumsen Memorial Foundation, The King Christian 10th Foundation, The Beckett Foundation, by Public Health Service Grants RO1-CA40303, RO1-HL39810, the Whitaker Foundation RO1-CA66072, and PO1-CA48729.

0740-3194/96 $3.00

the region is thus given by

$$C_V(t) = C_a(t) \otimes h(t) \equiv \int_0^t C_a(\tau)h(t-\tau)d\tau \quad [1]$$

where $\otimes$ denotes convolution. The MTT for the tracer particles is defined in terms of the density function:

$$\text{MTT} = \frac{\int_{-\infty}^{\infty} \tau h(\tau)d\tau}{\int_{-\infty}^{\infty} h(\tau)d\tau} \quad [2]$$

This equation has been used to determine flow under different assumptions about the relationship between MTT and the observed passage time of an intravascular contrast bolus (6). As pointed out by Weisskoff *et al.* (12), the distinction between this MTT and the first moment of the concentration time curve obtained from imaging of intravascular bolus passages is, however, crucial in attempts to measure absolute flow using intravascular tracers.

The amount of intravascular tracer in the VOI is determined by

$$\text{CBV} = \frac{\int_{-\infty}^{\infty} C_{\text{VOI}}(\tau)d\tau}{\int_{-\infty}^{\infty} C_a(\tau)d\tau} \quad [3]$$

In the case of brain tissue with an intact blood brain barrier (BBB), the distribution space of common paramagnetic NMR contrast agents is equal to the intravascular, extracellular space, i.e., the plasma volume. The fraction of tissue available for tracer distribution is thus $(1\text{-Hct}_m) \cdot \text{CBV}_f$, where Hct_m is the microvascular hematocrit and CBV_f is the cerebral full blood volume. Hct_m is a complicated function of vessel size, flow, and pathophysiological conditions but is generally 40–100% of the systemic blood hematocrit (13). The discussion of these effects is outside the scope of this paper. Throughout our simulations, values of CBF and CBV will refer to full blood flow, assuming a macrovascular to microvascular hematocrit ratio of 2/3 (13), independent of flow.

With the definition of MTT and CBV above, the central volume theorem (1, 2) states that the relationship between these and tissue flow, F_t

$$\text{MTT} = \frac{\text{CBV}}{F_t} \quad [4]$$

The central quantity in bolus-passage experiments is the fraction of injected tracer still present in the vasculature at time t, described by the *residue function* $R(t)$,

$$R(t) \equiv \left[1 - \int_0^t h(\tau)d\tau\right] \quad [5]$$

Note that by the definition of $h(t)$ as a probability density function, $R(0) = 1$ and $R(t)$ is a positive, decreasing function of time.

The concentration $C_{\text{VOI}}(t)$ of tracer within a given VOI can now be written

$$C_{\text{VOI}}(t) = F_t \int_0^t C_a(\tau)R(t-\tau)d\tau \quad [6]$$

Equation [6] is the central equation in our approach to determine flow using nondiffusible tracers. It states that the initial height of the deconvolved concentration time curve equals the flow, F_t. It is important to note that the arterial input function in Eq. [6] may undergo dispersion during its passage from the point of measurement to more peripheral tissue. This dispersion can be described mathematically as a convolution with a vascular transport function $h^*(t)$ (cf. Eq. [1]). If the residue function determined by using an arterial input that is subsequently dispersed is denoted $R^*(t)$ and the "true" residue function $R(t)$, using Eq. [6] would consequently yield $R^*(t) = h^*(t) \otimes R(t)$. The initial height of the deconvolved curve will thus be underestimated by the spread in $R^*(t)$. This underlines the importance of measuring the arterial input values close to the observed tissue to avoid dispersion.

Equation [6] is not straight forward to solve for F_t because $R(t)$ is an unknown function dependent on local vascular structure (10). This type of so-called *inverse problems* (14, 15), where integral equations are solved with respect to an unknown kernel, appears frequently in the biomedical literature, mainly in the context of venous output measurements (Eq. [1]). The basic principles in solving these equations are, however, generally applicable and in the following we will apply and refer to them in the context of vascular residue functions.

The approaches to deconvolve Eq. [6] are divided into two main categories. In *model dependent techniques*, we assume a specific analytical expression or the shape of $R(t)$. Assuming a specific shape for $R(t)$ imposes assumptions on the tissue microvasculature. For this reason, some have argued that Eq. [6] cannot be used to determine flow by deconvolution with an arterial input function in part since $R(t)$ cannot be known *a priori* with sufficient precision (10). This problem can, at least in theory, be circumvented by performing nonparametric deconvolution without *a priori* knowledge of $R(t)$. The latter *model independent* approach, where the flow *and* the shape of $R(t)$ are determined from the experiment by nonparametric deconvolution, forms the other main category of approaches to solve Eq. [6] for F_t and $R(t)$.

The goal of this work was to find the optimal deconvolution approach to allow determination of $R(t)$ and tissue flow from Eq. [6]. In the following, we describe how we modified and compared general model-dependent as well as model-independent approaches for the special requirements of CBF measurements using nondiffusible susceptibility tracers in MRI.

DECONVOLUTION TECHNIQUES

Model-Dependent (Analytical) Deconvolution

One reason for describing $R(t)$ with an analytical function is partly that it makes the deconvolution in Eq. [6] more stable since it reduces the degrees of freedom for the resulting shape or the shape of $R(t)$. To clarify the division of approaches in this paragraph, we use the term "deconvolution" to describe the determination of CBF and MTT from arterial and tissue concentration time curves by nonlinear least squared fitting, although this terminology should perhaps be reserved for the model-dependent approaches below. This approach introduces the assumption that the actual vascular structure can be described by a particular function.

Exponential decrease has been proposed as a general model for tissue residue functions. This is based on a simple model of the vascular bed as one single, well-mixed compartment. For such a system, the residue function is an exponential (16, 17). Taking into account more complicated models of capillaries including the effects of "plug" flow (the fact that the red blood cells fill the capillary lumen completely and thus to some extent prevent mixing), it has been argued that a linear combination of a finite number of exponentials still may be an appropriate model for the residue function (11).

We used a single exponential as a first-order model to describe the residue function:

$$R(t, \mathrm{MTT}) = e^{-\frac{t}{\mathrm{MTT}}} \qquad [7]$$

We used general nonlinear least squared minimization to fit for MTT and F_t (15).

Model-Independent (Nonparametric) Deconvolution

In this approach, $R(t)$ is determined along with F_t. Equations [1] and [6] are, with respect to $R(t)$, both Fredholm integral equations of the first kind (14, 15). These equations are generally unstable in the sense that infinitesimal changes (in our case noise) in $C_{\mathrm{VOI}}(t)$ give rise to finite changes in $R(t)$. The techniques described below mainly differ in the way they moderate the effects of noise in the measurements. The techniques fall into two subcategories: In the first, *transform* approach, the convolution theorems for the Fourier, Z, or Laplace transforms are used to deconvolve Eq. [6]. In the second, *algebraic* approach, Eq. [6] is rewritten as a matrix equation and solved.

These techniques have mainly been applied at high SNR to find residue or transport functions with long MTTs compared with the temporal resolution of the experiments. In the following, we will focus on modifications necessary for our applications, finding CBF using dynamic MRI of bolus passages.

Transform Approach. In this approach, the convolution theorem of the Laplace, Z, or Fourier transform (FT) is used (7, 8, 18–21). Denoting by $F\{\}$ the Fourier transform (FT), the convolution theorem states that $F\{\}$ is multiplicative to convolution. Equation [6] thus becomes:

$$F\{C_{\mathrm{VOI}}(t)\} = F_t \cdot F\{C_a(t) \otimes R(t)\} = F_t \cdot F\{C_a(t)\} \cdot F\{R(t)\} \qquad [8]$$

or in other words,

$$R(t) = F_t^{-1}\, F^{-1}\left\{\frac{F\{C_{\mathrm{VOI}}(t)\}}{F\{C_a(t)\}}\right\} \qquad [9]$$

where $F^{-1}\{\}$ denotes the inverse FT. The residue function and flow can thus be determined by taking the inverse FT of the ratios of two transforms at every time point of the known arterial input and tissue time-activity curve. This approach is—in this form—very sensitive to noise. The FT of the arterial and cerebral curves, however, yield a frequency representation of the data where noise is represented at high frequencies, whereas "real" physiological signal has higher power at lower frequency. This allows one in principle to apply a filter that retains "physiological" frequencies but damps noise before performing the inverse Fourier transform to determine $F_t \cdot R(t)$. We implemented an automated filtering procedure described by Gobbel and Fike (7), which is a modified version of the Wiener filter (15), increasing the stength of the filter until a global constraint on the degree of oscillations was fulfilled. Rempp *et al.* (8) also reported using an optimal Wiener filter for deconvolution of tissue concentration time curves to determine flow.

Algebraic Approach. This approach is based on an algebraic reformulation of the convolution integrals in Eqs. [1] and [6] and has been used extensively in the analysis of tracer transport functions (22–26).

Assume that the arterial and cerebral concentrations are measured at a set of equally spaced time points $t_1, t_2, \ldots, t_N$. Assume that, over small time intervals, the residue function and arterial input values are constant. The convolution in Eq. [6] can then be formulated as a matrix equation (22):

$$C(t_j) = \int_0^{t_j} C_a(\tau)R(t-\tau)d\tau \approx \Delta t \sum_{i=0}^{j} C_a(t_i)R(t_j - t_i) \qquad [10]$$

or

$$\Delta t \begin{pmatrix} C_a(t_1) & 0 & \cdots & 0 \\ C_a(t_2) & C_a(t_1) & \cdots & 0 \\ \cdots & \cdots & \cdots & \cdots \\ C_a(t_N) & C_a(t_{N-1}) & \cdots & C_a(t_1) \end{pmatrix} \cdot \begin{pmatrix} R(t_1) \\ R(t_2) \\ \cdots \\ R(t_N) \end{pmatrix} = \begin{pmatrix} C_{br}(t_1) \\ C_{br}(t_2) \\ \cdots \\ C_{br}(t_N) \end{pmatrix} \qquad [11]$$

In the following we shall use the short-hand vector notation

$$A \cdot \mathbf{b} = \mathbf{c} \qquad [12]$$

for this equation, where $\mathbf{b}$ contains the elements of $R(t_i)$, $i = 1,2,\ldots,N$, and $\mathbf{c}$ are the measured cerebral tracer concentrations (22–26). Note that Eq. [11] can be solved iteratively for the elements of $\mathbf{b}$. This approach is, however, extremely sensitive to noise, causing $R(t)$ to oscillate. Solving Eq. [12] thus involves minimizing the effects of noise and at the same time minimizing

$$|A \cdot \mathbf{b} - \mathbf{c}| \qquad [13]$$

where $|\ |$ denotes the vector norm.

The algebraic approach has been used extensively in the analysis of tracer transport functions and residue functions in organs with relatively long MTTs. The technique assumes that arterial and tissue concentrations are constant between measurements. In the context of rCBF measurements using dynamic MR imaging of intravascular bolus passages, both the arterial input function and the residue function are expected to vary over small time scales compared with the temporal resolution of the measurements (1–1.5 s for typical spin-echo EPI imaging). The constancy of these functions between measurements is thus a poor approximation. In our approach we assumed that $C_a(t)$ and $R(t)$ both vary *linearly* with time. It can be shown that the elements a_{ij} of the matrix A in Eq. [11] become

$$a_{ij} = \begin{cases} \Delta t(C_a(t_{i-j-1}) + 4 \cdot C_a(t_{i-j}) + C_a(t_{i-j+1}))/6 & 0 \le j \le i \\ 0 & \text{else} \end{cases} \quad [14]$$

In our work, then, this matrix was used for A when solving Eq. [13].

Regularization. A widely used approach to solve Eq. [13] is *regularization*, minimizing

$$|A \cdot \mathbf{b} + \mathbf{f}(\mathbf{b}) - \mathbf{c}| \quad [15]$$

rather than Eq. [13], where $\mathbf{f}(\mathbf{b})$, the regularization term, is a function of $\mathbf{b}$. By appropriately choosing $\mathbf{f}$, the solution $\mathbf{b}$ can be constrained to be mathmatically "well-behaved" and at the same time be physiologically meaningful. Regularization, in a biological context, has mainly been applied to determine transport functions (cf. Eq. [1]). Existing regularization approaches are thus not applicable for our purpose, determining residue function. The major drawback of regularization is that, like analytical deconvolution, it creates a result that matches *a priori* expectations of the shape of $\mathbf{b}$ at the expense of the the quality of the fit to the actual data (15).

We implemented a regularization term modified for finding residue functions without significantly affecting the fit to experimentally determined data. The regularization term $\mathbf{f}(\mathbf{b})$ imposes a mild constraint on $R(t)$ of being a decreasing function of time:

$$f_j(\mathbf{b}) = \begin{cases} P_{\text{REG}} \cdot (b_j - b_{j-1}) & \text{if } b_j < 1.1 \cdot b_{j+1} \\ 0 & \text{else} \end{cases} \quad [16]$$

where P_{REG} is a free parameter. Increasing P_{REG}'s size allows one to strengthen the constraint on $R(t)$ of being a decreasing function of time relative to that of solving Eq. [9]. This regularization term has the advantage of disappearing when $R(t)$ is a decreasing function of time and thus will not affect the quality of the fit as long as this single physiological constraint is fulfilled. We solved Eq. [15] for the elements of $R(t_j)$ by least squared minimization (15).

Singular Value Decomposition (SVD). Another technique to solve Eq. [12] uses the SVD. Apart from changing the matrix A in Eq. [11] for the use with rapidly varying functions of time, we did not modify the SVD technique. We will thus restrict ourselves to a brief general description of the technique.

The SVD constructs matrices V, W, and U^T so that the inverse of A in Eq. [12], A^{-1}, can be written:

$$A^{-1} = V \cdot W \cdot U^T \quad [17]$$

where W is a diagonal matrix (i.e., off-diagonal elements are zero). V and U^T are orthogonal and transpose orthogonal matrices (i.e., have orthogonal, unit length columns), respectively. Given this inverse matrix, $\mathbf{b}$, and consequently $R(t)$, is found simply as

$$\mathbf{b} = V \cdot W \cdot (U^T \cdot \mathbf{c}) \quad [18]$$

The main force of the SVD is that the diagonal elements in W are zero or close to zero corresponding to linear equations in Eq. [11] that are close to being linear combinations of each other. This fact thus allows one to identify elements in the matrix A that causes the solution $\mathbf{b}$ to oscillate or otherwise be meaningless in a biomedical modeling context. In terms of sampling data from bolus passage experiments, the fact that equations in Eq. [11] are close to being linear combinations of each other means that data are being sampled at time points where changes in arterial or cerebral concentration time curves over time are small relative to the noise. By eliminating (setting equal to zero) diagonal elements below a certain threshold in W, one can consequently minimize these effects before calculating $\mathbf{b}$. The resulting $\mathbf{b}$ (after elimination of diagonal elements) can be shown to be the best possible solution of Eq. [13] in a least squared sense (15). For more detail, see Press *et al.* (15) and Van Huffel *et al.* (26) and references therein.

SIMULATION SCHEME

We performed a series of Monte Carlo simulations to determine the performance of the deconvolution techniques under different physiological characteristics and SNRs. We first describe the arterial input and the physiological characteristics of the vascular bed used in our simulations, and then describe how the nonparametric deconvolution techniques used were optimized at each SNR before our simulations.

Simulated Arterial Input

For our simulations, we used an arterial input with a shape and size that could typically be obtained using a standard injection scheme. This was done by adjusting the parameters of a gamma variate function combined with a dispersion term to resemble the averaged arterial bolus size and shape observed around large vessels in six normal volunteers participating in clinical testing (27) of Sprodiamide (Nycomed Inc., Princeton, NJ, and Nycomed Imaging AS, Oslo, Norway). The resulting analytical expression was:

$$C_a(t) \propto \begin{cases} 0 & t \le t_0 \\ (t - t_0)^{3.0} \cdot e^{-\frac{t}{1.5\,s}} & t > t_0 \end{cases} \quad [19]$$

where t_0 is the tracer arrival time. The subsequent recirculation was modeled to have a delay of 8 s and a dispersion with a time constant of 30 s. This was achieved

slice. Table 2 summarizes the main features of the different ASL techniques, which are described more fully in the following paragraphs.

Echo planar imaging and signal targeting with alternating radiofrequency. The first of the PASL group of perfusion imaging approaches was proposed by Edelman et al. in 1994 and is known as echo planar imaging and signal targeting with alternating radiofrequency (EPISTAR) (Edelman et al., 1994). This technique is similar conceptually to CASL. After saturation of the imaging slice (see Transit Time Effects later), a slab proximal to the imaging slice is labeled using a single, short RF inversion pulse. The blood in this slab then is allowed to flow into the imaging slice, and an image is acquired after a time TI. A control image also is acquired for which the label is applied distal to the imaging slab (Edelman et al., 1994) or with no slab selective gradient (a variant known as PICORE [proximal inversion with control for off-resonance effects, Wong et al., 1997]). Recently, in an approach similar in concept to that of Alsop and Detre for CASL described in the previous section, the control image was acquired by applying a "double inversion" pulse pair (Edelman and Chen, 1998). The MT effect on the imaging slices is the same in the control and spin labeled images, and inflowing blood in the control image is fully relaxed, since it experiences an overall 0° nutation. Subtraction of the images results in a flow-dependent image with a signal intensity determined by (Kwong et al., 1995; Calamante et al., 1996):

$$\Delta M = 2M_0 \cdot TI \cdot \left(\frac{f}{\lambda}\right)\exp\left(-\frac{TI}{T_1}\right) \qquad (13)$$

where ΔM is the difference in magnetization per unit mass between the labeled and control images, M_0 is the equilibrium tissue magnetization per unit mass of tissue, and TI is the time between spin inversion and image acquisition (inversion time). This theoretical signal difference is less than that of CASL by a factor of $exp(-TI/T_1)$. Equation 13 relies on several simplifying assumptions, such as tissue and blood T_1 being equal and the efficiency of the inversion pulse being equal to 1. Under practical circumstances these assumptions are not valid, and a more general analysis (Calamante et al., 1996) predicts a biexponential relation between ΔM and TI:

$$\Delta M = 2\alpha_0 M_0 \frac{f}{\lambda}\left[\frac{\exp\left(-\frac{TI}{T_{1app}}\right)-\exp\left(-\frac{TI}{T_{1a}}\right)}{\frac{1}{T_{1a}}-\frac{1}{T_{1app}}}\right] \qquad (14)$$

where α_0 is the degree of inversion of the spin labeling pulse and T_{1app} is defined in Eq. 9. If $T_{1a} \sim T_{1b}$ and α_0 is unity, Eq. 14 reduces to Eq. 13. However, for

TABLE 2. *Principal classifications of the arterial spin labeling techniques*

Technique	CASL or PASL	Tagged experiment	Control experiment	Tagged experiment (schematic)	Control experiment (schematic)	Notes
Steady-state/ continuous	CASL	Proximal AFP inversion at level of feeding arteries	Distal AFP inversion			Post-labeling (w) delay reduces δ-sensitivity; AM control or 2-coil technique allows multislice acquisition
FAIR	PASL	Slice-selective inversion	Non–slice-selective inversion			Amenable to multislicing; susceptible to slice profile imperfections
UNFAIR	PASL	Non-selective followed by a selective inversion	Dual non-selective inversion (360°)			See FAIR
EPISTAR	PASL	Proximal slab inversion	Distal slab inversion or double inversion			See FAIR
PICORE	PASL	Proximal slab inversion	Inversion pulse applied without selective gradient			See FAIR
QUIPSS/ QUIPSS II	PASL	Bolus time-width defined by saturation pulse in the imaging (QUIPSS) or labeled region (QUIPSS II) of the above pulse sequences		See Fig. 1 in (Wong et al., 1998*a*)		Generic means of reducing δ-sensitivity of the PASL techniques

δ denotes the transit time. The schematic representations of the experiments are shown relative to a sagittal view of the brain. The dashed lines represents the area of the imaging slice; ▨ depicts the inverted area and ▩ denotes the presaturation of the imaging slice. The schematic representation of the CASL tagging experiment displays a labeling plane that intersects the carotid arteries.

AFP, adiabatic fast passage; AM, amplitude modulated; CASL, continuous arterial spin labeling; EPISTAR, echo planar imaging and signal targeting with alternating radiofrequency; FAIR, flow-sensitive alternating inversion recovery; PASL, pulsed arterial spin labeling; PICORE, proximal inversion with control for off-resonance effects; QUIPSS, quantitative imaging of perfusion using a single subtraction; UNFAIR, uninverted flow-sensitive alternating inversion recovery.

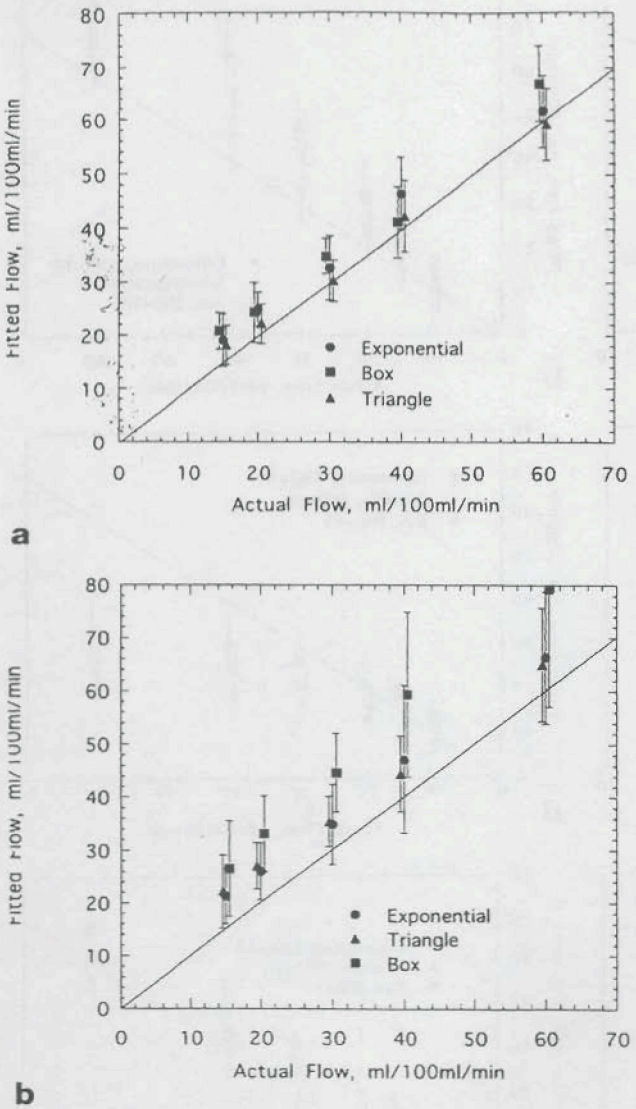

FIG. 2. Reproduction of flow values for different underlying residue functions for the regularization (a) and SVD (b) approaches, respectively, at SNR = 10. In this case, vascular volume was 4.5%. Note that the flows fitted by regularization approach show a strong dependence on CBV, whereas this was less prominent with the SVD approach (compare with Figs. 1f and 1h). The high flow values seem to be less underestimated at this volume than in the case of a CBV of 3.0% (Fig. 1h).

Table 1
Summary of Monte Carlo Modeling Results

Deconvolution approach	Flow estimate independence of		
	Vascular structure	CBF	CBV
Model dependent (exponential)	÷		
Fourier transform	+	÷	
Regularization	+	+	÷
SVD	+	+	+

Flow estimate independence of a given quantity is indicated by +, dependence by ÷.

was a general finding of our simulations that there was no sudden loss of the degree to which the fitted curves reflected the underlying true residue function. Rather, the shape changed from that of the true underlying residue function to a smooth curve with only few of the details of the underlying residue function.

The regularization approach (Fig. 4b) generally showed a tendency to change the fitted residue function into a triangular shape when going toward lower SNR. This is probably due to the constraint imposed by the regularization term, favoring this shape. Also, each point of the fitted $R(t)$ was determined with increased uncertainty at the lower SNR. We believe this bias toward a triangular shape is the cause of the overestimation of flow noticed for regularization approach in Fig. 2a.

Generally, using the SVD, at a SNR of below 50–100, the noise on each point on the determined underlying residue function was too large to yield qualitative information on the underlying curve. For the regularization approach, higher SNR was found to be necessary to determine the shape of the residue function.

DISCUSSION

Our simulations clearly demonstrate the potential dangers of using simplified assumptions when modeling the vascular residue function. Assuming a simple, mono-exponential residue function will thus introduce large systematic errors when flows in two regions with different residue functions are compared. This is in line with the conclusions made by Lassen (10) and Weisskoff *et al.* (12). We performed simulations to evaluate if using a multi-exponential residue model improved the reproduction of flow. The introduction of extra parameters, however, did not change this general conclusion. This result is a drawback to the choice of the exponential as a first approximation to the residue function in the model-dependent approach. In a companion paper (31), we qualitatively analyze other simple, analytical expres-

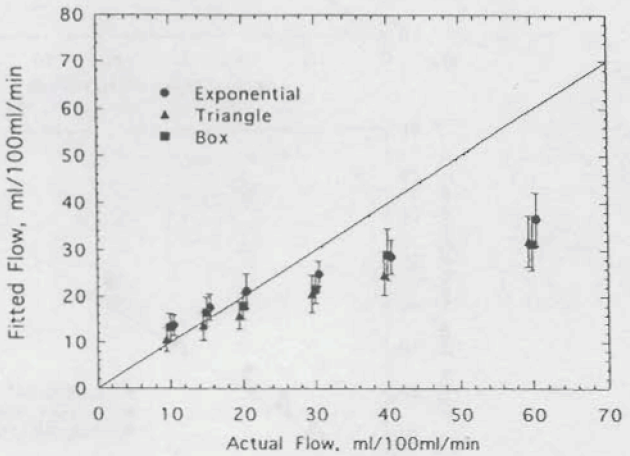

FIG. 3. Reproduction of flow at a CBV of 3.0% and the SVD model-independent deconvolution approach. The tissue concentration time curve was delayed by 2 s relative to the arterial input. Note how this causes substantial underestimation of flow at high flow values, whereas low flow rates are still well reproduced.

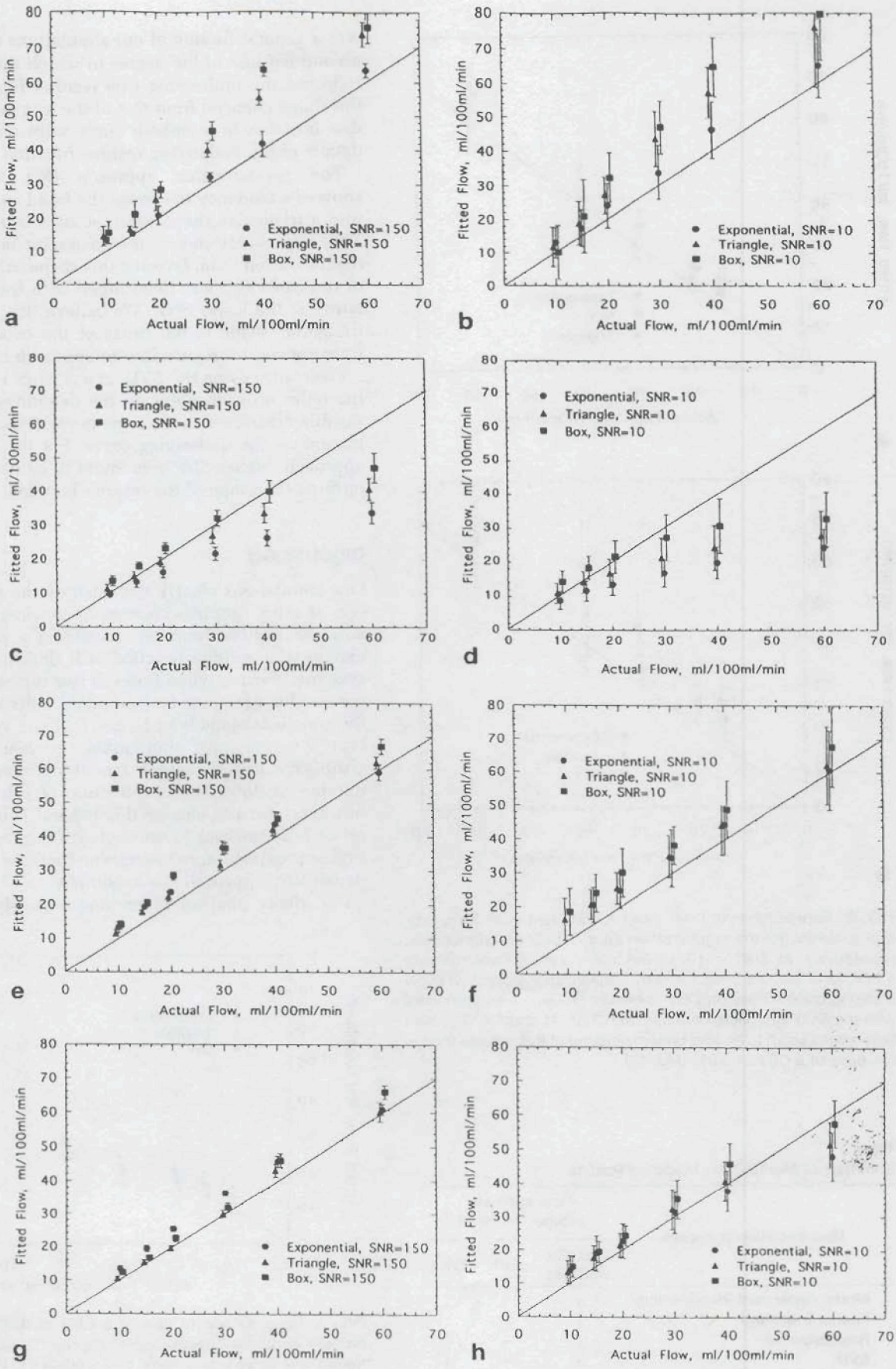
a
Fitted Flow, ml/100ml/min
Actual Flow, ml/100ml/min
Exponential, SNR=150
Triangle, SNR=150
Box, SNR=150
b
Exponential, SNR=10
Triangle, SNR=10
Box, SNR=10
c
d
e
f
g
h

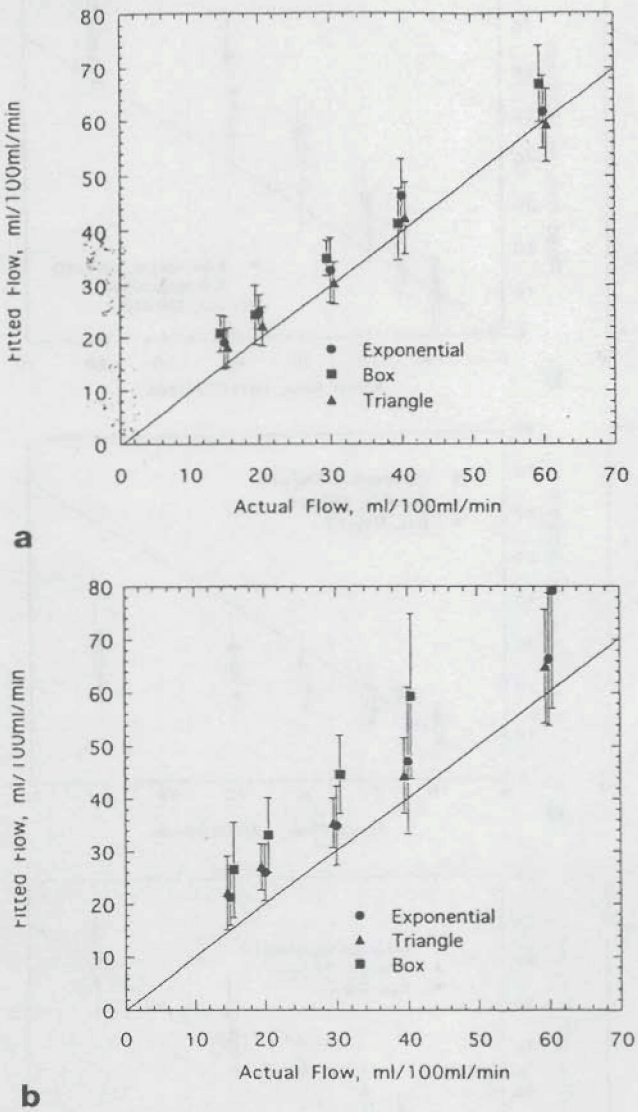

FIG. 2. Reproduction of flow values for different underlying residue functions for the regularization (a) and SVD (b) approaches, respectively, at SNR = 10. In this case, vascular volume was 4.5%. Note that the flows fitted by regularization approach show a strong dependence on CBV, whereas this was less prominent with the SVD approach (compare with Figs. 1f and 1h). The high flow values seem to be less underestimated at this volume than in the case of a CBV of 3.0% (Fig. 1h).

Table 1
Summary of Monte Carlo Modeling Results

Deconvolution approach	Flow estimate independence of		
	Vascular structure	CBF	CBV
Model dependent (exponential)	÷		
Fourier transform	+	÷	
Regularization	+	+	÷
SVD	+	+	+

Flow estimate independence of a given quantity is indicated by +, dependence by ÷.

was a general finding of our simulations that there was no sudden loss of the degree to which the fitted curves reflected the underlying true residue function. Rather, the shape changed from that of the true underlying residue function to a smooth curve with only few of the details of the underlying residue function.

The regularization approach (Fig. 4b) generally showed a tendency to change the fitted residue function into a triangular shape when going toward lower SNR. This is probably due to the constraint imposed by the regularization term, favoring this shape. Also, each point of the fitted $R(t)$ was determined with increased uncertainty at the lower SNR. We believe this bias toward a triangular shape is the cause of the overestimation of flow noticed for regularization approach in Fig. 2a.

Generally, using the SVD, at a SNR of below 50–100, the noise on each point on the determined underlying residue function was too large to yield qualitative information on the underlying curve. For the regularization approach, higher SNR was found to be necessary to determine the shape of the residue function.

DISCUSSION

Our simulations clearly demonstrate the potential dangers of using simplified assumptions when modeling the vascular residue function. Assuming a simple, mono-exponential residue function will thus introduce large systematic errors when flows in two regions with different residue functions are compared. This is in line with the conclusions made by Lassen (10) and Weisskoff *et al.* (12). We performed simulations to evaluate if using a multi-exponential residue model improved the reproduction of flow. The introduction of extra parameters, however, did not change this general conclusion. This result is a drawback to the choice of the exponential as a first approximation to the residue function in the model-dependent approach. In a companion paper (31), we qualitatively analyze other simple, analytical expres-

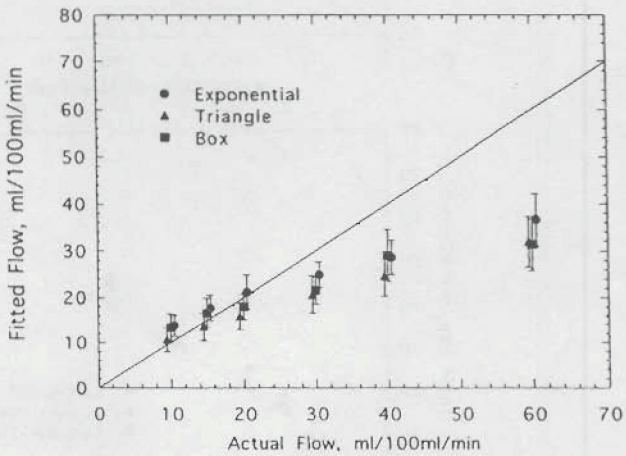

FIG. 3. Reproduction of flow at a CBV of 3.0% and the SVD model-independent deconvolution approach. The tissue concentration time curve was delayed by 2 s relative to the arterial input. Note how this causes substantial underestimation of flow at high flow values, whereas low flow rates are still well reproduced.

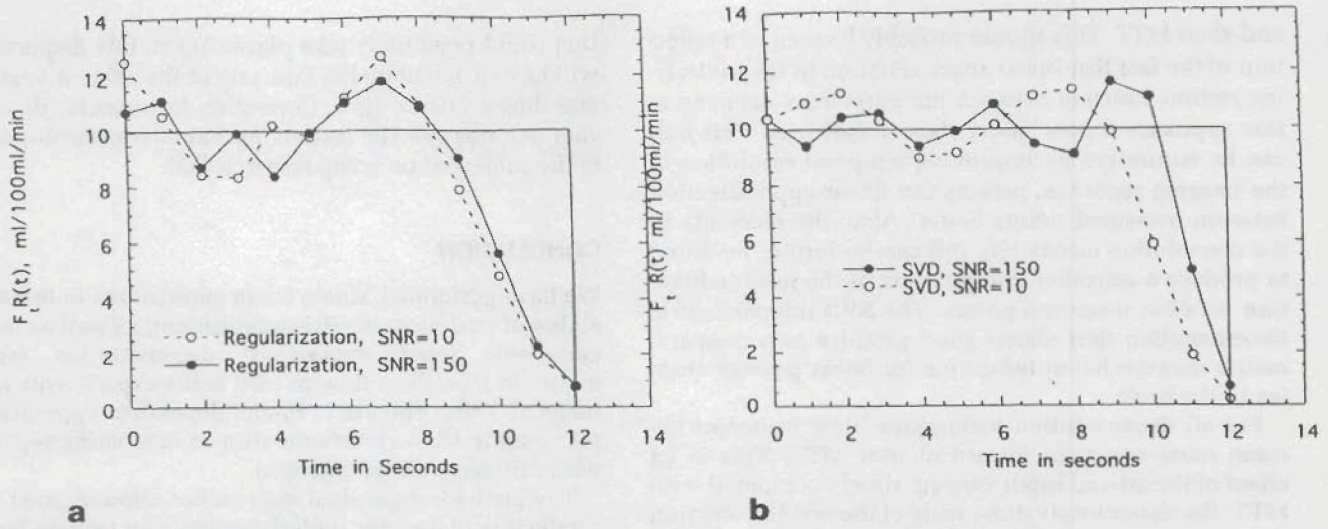

FIG. 4. (a) Optimized reproduction of the underlying residue function for the SVD nonparametric deconvolution technique at two differen noise levels, SNR = 150 and SNR = 10. The solid line indicates the true, underlying residue function. Note that the shape gradually looses resemblance to the underlying residue function going toward lower SNR. CBV was 3.0%. (b) Optimized reproduction of the underlying residue function for the regularization nonparametric deconvolution technique at two different noise levels, SNR = 150 and SNR = 10 The solid line indicates the true, underlying residue function. Note that the shape tends to become more triangular as the SNR decreases reflecting the underlying regularization term. CBV was 3.0%.

sions to characterize the cerebral residue function. Models including very detailed models of vascular transport and exchange have been proposed (33). Further work is needed to provide operators that describe a wide variety of vascular residue functions in the brain.

Of nonparametric deconvolution techniques evaluated, the Fourier transform failed to reproduce F_t at short MTTs just as it showed a dependency on the the underlying residue function. These facts are both reflections of the properties of the FT in the physiological context in which we applied it. Even in the absence of noise, the FT gives approximately $F_t/2$ at the initial point of the response function. The flow is thus estimated from the following point on the response curve. This has two effects. First, for relatively short MTTs compared with the sampling rate, the impulse response function will have decayed substantially at the first sample of the residue function, leading to underestimation of flow as we found in our simulations. Secondly, the degree of decay of the response function before the second sample is dependent on the residue model. In agreement with this, flow was most severely underestimated for the most rapidly decreasing residue model, namely the exponential. Furthermore, applying filters to improve the SNR of the measurement introduces a blurring in the time domain, causing the maximum point on the response curve to be further underestimated. This was demonstrated in our simulations by the more severe underestimation of flow at low SNR where more powerful filtering had been applied.

The underestimation of flow for short MTTs relative to the sampling rate has severe implications for determination of flow using FT. In comparing two regions with equal actual flow, the region with the highest CBV (and thus longest MTT) will appear to have a higher flow rate using the FT, making the estimates biased by the rCBV. The FT approach is thus misleading in evaluating states of high flow and short MTT unless the sampling rate ca be improved relative to the MTTs in question. Interest ingly, the use of an unmodified Wiener filter, may not b optimal in finding residue functions. The Wiener filter i designed to minimize the mean square error over all tim whereas we, for estimates of flow, wish to minimize th errors in just the initial value of the residue function Because of these differences, the use of a true Wiene filter would produce large underestimations flow. I light of these theoretical concerns, we compared simula tion results obtained with the modified Wiener filter (6 to similar results obtained with a Hanning filter afte optimization to yield similar standard deviations of th flow estimates. We got comparable reproduction of flo rates for the two approaches, demonstrating that th modifications to the Wiener filter approach by Gobbel *et al* (6) compensate for the theoretical draw-backs men tioned above.

Nonparametric deconvolution using regularizatio could be optimized to yield good reproduction of flo However, subsequent use of the technique at a differe rCBV showed some dependence on vascular volume. W believe this effect should be seen as a result of the fa that changing CBV effectively changes the SNR of th concentration time curve. Since the optimization of th regularization is dependent on the SNR, one choice this optimization may not suffice to optimize the repr duction of flow for all values of CBV, thus introducir the observed bias on flow rates. More optimal regulariz tion terms than the one we used here may improve th technique.

The SVD nonparametric deconvolution technique— contrast to the other model-independent approaches showed an excellent ability to reproduce flow with go accuracy independent of the underlying vascular stru ture and volume. The bias of underlying residue functi increased somewhat toward combinations of high flo

and short MTT. This should probably be seen as a reflection of the fact that linear approximation to the underlying residue function between measurements assumed in this approach is poor under these conditions. This bias can be minimized by improving temporal resolution of the imaging sequence, making the linear approximation between measured points better. Also, the elements in the convolution matrix (Eq. [8]) can be further modified to produce a smoother interpolation of the residue function between measured points. The SVD nonparametric deconvolution thus shows good promise as a nonparametric deconvolution technique for bolus passage studies in the brain.

For all deconvolution techniques, flow estimates became more uncertain toward shorter MTT. This is an effect of the arterial input varying slowly compared with MTT, the characteristic time scale of the residue function that we want to sample. Note that the characteristic time scale of the arterial input used in our simulations is roughly 1.5 s (Eq. [19]). This general constraint can only be circumvented by using rapid bolus injections to create very sharp arterial input profiles.

The ability of nonparametric deconvolution techniques to reproduce the *shape* underlying residue function $R(t)$ was generally poorer than the ability to reproduce flow. Model-independent approaches in our simulations required high SNR (50–100 with a typical contrast injection, imaging sequence and resolution in the brain) to reproduce the tissue residue function. This should be compared with the pixel-by-pixel SNR of about 10 in our actual imaging experiments. Performing regional rather than pixel-by-pixel deconvolution will thus still provide mostly qualitative information on the shape of the residue function just as tissue heterogeneity will cause a loss of specific, localized information. This technique thus awaits the development of more potent contrast agents and ways of obtaining higher SNR in human studies of $R(t)$. In an experimental setting, however, animal experiments at high field using iron oxide contrast agents may provide sufficient SNR and contrast-to-noise ratio (CNR) to allow high resolution studies of $R(t)$ with this technique. This may, in turn, provide important information on vascular structure and reactivity in normal as well as pathological brain tissue.

Our analysis shows that delays between arterial input and the tissue response are important in accurately determining flow. It is important to note that tracer arrival delays often occurs in states where flow is low, for example as a result of collateral circulation in the periphery of stroke areas. In these situations, our simulations indicate that flow will only be slightly underestimated. In regions of high flow, high flow rate in the afferent vessels will tend to create a relatively shorter delay. On the other hand, understimation of tissue flow were shown to be more severe, and delays should consequently be corrected during image analysis by either fitting the delay as a free parameter (model-dependent approach) or independent determination of the tracer arrival delays (model-independent approaches). We are presently investigating methods for performing this correction. Also, it should be noted that the pathologies mentioned above are examples where dispersion of the arterial input function could potentially take place. Again, this dispersion will be dependent on the flow rate in the afferent vessels and thus on tissue flow. Correction for vascular dispersion requires specific models for vascular transport and is the subject of on-going research (33).

CONCLUSION

We have performed Monte Carlo simulations to test the ability of analytical (model-independent) as well as nonparametric (model-dependent) deconvolution techniques to reproduce flow in MRI bolus experiments at a range of SNRs. The use of model-dependent approaches may lead to large systematic error in comparing regions with different residue function.

The model-independent approaches allowed good reproduction of the true, underlying vascular residue function only at high SNR. Toward lower SNR, the fitted residue functions were in mere qualitative agreement with the actual, underlying residue function.

We demonstrated that SVD is able to reproduce flow with good accuracy relatively independent of the underlying vascular structure even at the SNR typical of pixel-by-pixel deconvolution after 3-by-3 uniform filtering of the images. This approach thus shows promise as an approach to high resolution model-independent determination of CBF using dynamic imaging of paramagnetic bolus passages in humans.

REFERENCES

1. G. N. Stewart, Researches on the circulation time in organs and on the influences which affect it. Parts I-III. *J. Physiol. (London)* **15**, 1 (1894).
2. P. Meier, K. L. Zierler, On the theory of the indicator-dilution method for measurement of blood flow and volume. *Appl. Physiol* **6**, 731–744 (1954).
3. L. Axel, Cerebral blood flow determination by rapid-sequence computed tomography. *Radiology* **137**, 679–686 (1980).
4. B. R. Rosen, J. W. Belliveau, J. M. Vevea, T. J. Brady, Perfusion imaging with NMR contrast agents. *Magn. Reson. Med.* **14**, 249–265 (1990).
5. B. R. Rosen, J. W. Belliveau, B. R. Buchbinder, R. C. McKinstry, L. M. Porkka, D. N. Kennedy, M. S. Neuder, C. R. Fisel, H. J. Aronen, K. K. Kwong, R. M. Weisskoff, M. S. Cohen, T. J. Brady, Contrast agent and cerebral hemodynamics. *Magn. Reson. Med.* **19**, 285–292 (1991).
6. G. T. Gobbel, C. E. Cann, J. R. Fike, Measurement of regional cerebral blood flow using ultrafast computed tomography. Theoretical aspects. *Stroke* **22**, 768–771 (1991).
7. G. T. Gobbel, J. R. Fike, A deconvolution method for evaluating indicator-dilution curves. *Phys. Med. Biol.* **39**, 1833–1854 (1994).
8. K. A. Rempp, G. Brix, F. Wenz, C. R. Becker, F. Guckel, W. J. Lorenz, Quantification of regional cerebral blood flow and volume with dynamic susceptibility contrast-enhanced MR imaging. *Radiology* **193**, 637–641 (1994).
9. N. Wilke, K. Kroll, H. Merkle, Y. Wang, Y. Ishibashi, Y. Xu, J. Zhang, M. Jerosch-Herold, A. Mühler, A. E. Stillman, J. B. Bassingthwaighte, R. Bache, K. Ugurbil, Regional myocardial blood volume and flow: first-pass MR-imaging with polylysine-Gd-DTPA. *J. Magn. Reson. Imaging* **5**, 227–237.
10. N. A. Lassen, Cerebral transit of an intravascular tracer may allow measurement of regional blood volume but not regional flow. *J. Cereb. Blood Flow Metabol.* **4**, 633–634 (1984).
11. J. A. Jacquez, *in* "Compartmental Analysis in Biology and Medicine. Kinetics of distribution of tracer-labeled materials," pp. 84–101, Elsevier Publishing Company, Amsterdam, 1972.
12. R. M. Weisskoff, D. Chesler, J. L. Boxerman, B. R. Rosen, Pitfalls in MR measurements of tissue blood flow with intravascular tracers: which mean transit time? *Magn. Reson. Med.* **29**, 553–559 (1993).

13. O. A. Larsen, N. A. Lassen, Cerebral haematocrit in normal man. *J. Appl. Physiol.* **19(4)**, 571–574 (1964).
14. G. M. Wing, *in* "A Primer on Integral Equations of the First Kind. The Problem of Deconvolution and Unfolding." SIAM Publishing Company, Santa Fe, NM, 1991.
15. W. H. Press, S. A. Teukolsky, W. T. Vetterling, B. T. Flannery, *in* "Numerical Recipes in C. The Art of Scientific Computing," 2nd ed., Cambridge University Press, Oxford, 1992.
16. J. B. Bassingthwaighte, C. A. Goresky, *in* "Handbook of Physiology Section 2: The Cardiovascular System" (E. M. Renkin, C. G. Michel, Eds.), pp. 549–626, American Physiology Society, Bethesda, 1984.
17. N. A. Lassen, O. Henriksen, P. Sejrsen, *in* "Handbook of Physiology Section 2: The Cardiovascular System" (J. T. Shepherd, F. M. Abboud, Eds.), pp. 21–64, American Physiology Society, Bethesda, 1984.
18. C. M. Coulam, H. R. Warner, H. W. Marshall, J. B. Bassingthwaighte, A steady-state transfer function analysis of portions of the circulatory system using indicator dilution techniques. *Comput. Biomed. Res.* **1**, 124–138 (1967).
19. C. M. Coulam, H. R. Warner, E. H. Wood, J. B. Bassingthwaighte, A Transfer function analysis of coronary and renal circulation calculated from upstream and downstream indicator-dilution curves. *Circ. Res.* **19**, 879–890 (1966).
20. C. I. I. I. Wall, H. S. Borovetz, J. J. Murphy, R. L. Hardesty, System parameter identification in transport models using the fast Fourier transform (FFT). *Comput. Biomed. Res.* **14**, 570–581 (1981).
21. J. B. Bassingthwaighte, Blood flow and diffusion through mammalian organs. *Science* **167**, 1347–1353 (1970).
22. M. E. Valentinuzzi, E. M. M. Volachec, Discrete deconvolution. *Med. Biol. Eng.* **13**, 123–125 (1975).
23. A. Todd-Pokropek, *in* "Cerebral Blood Flow. Mathematical Models, Instrumentation, and Imaging Techniques (A. Rescigno, A. Boicelli, Eds.), pp. 107–119, Plenum Press, New York, 1988.
24. T. A. Bronikowski, C. A. Dawson, J. H. Linehan, Model-free deconvolution techniques for estimating vascular transport functions. *Int. J. Biomed. Comput.* **14**, 411–429 (1983).
25. J. Bock, P. Deuflhard, A. Hoeft, H. Korb, H.-G. Wolpers, J. Steinman, G. Hellige, Thermal recovery after passage of the pulmonary circ tion of the pulmonary circulation assessed by deconvolution. *J. A Physiol.* **64**, 1210–1216 (1988).
26. S. Van Huffel, J. Vandewalle, M. C. De Roo, J. L. Willems, Reli and efficient deconvolution technique based on total linear l squares for calculating the renal retention function. *Med. Biol. E Comput.* **25**, 26–33 (1987).
27. A. G. Sorensen, S. M. Kulke, R. M. Weisskoff, J. L. Boxerman, B Buchbinder, B. R. Rosen, Investigation of cerebral hemodynam with sprodiamide (Dy-DTPA-BMA) and functional magnetic re nance imaging, *in* "Proc., ASNR, Nashville, 1994", p. 237.
28. A. Villringer, B. R. Rosen, J. W. Belliveau, J. L. Ackerman, R. Lauffer, R. B. Buxton, Y.-S. Chao, V. J. Wedeen, T. J. Brady, Dynar imaging with lanthanide chelates in normal brain: contrast due magnetic susceptibility effects. *Magn. Reson. Med.* **6**, 164–174 (19
29. R. M. Weisskoff, C. S. Zuo, J. L. Boxerman, B. R. Rosen BR, Mic scopic susceptibility variation and transverse relaxation: theory a experiment. *Magn. Reson. Med.* **31**, 601–610 (1994).
30. C. R. Fisel, J. L. Ackerman, R. B. Buxton, L. Garrido, J. W. Bellive B. R. B. R. Rosen, T. J. Brady, MR contrast due to microscopica heterogeneous magnetic susceptibility: numerical simulations a applications to cerebral physiology. *Magn. Reson. Med.* **17**, 348–3 (1991).
31. L. Østergaard, A. G. Sorensen, K. K. Kwong, R. M. Weisskoff, Gyldensted, B. R. Rosen. High resolution measurement of cereb blood flow using intravascular tracer bolus passages. Part II: Exp mental comparison and preliminary results. *Magn. Reson. Med.* 726–736 (1996).
32. K. L. Leenders, D. Perani, A. A. Lammertsma, J. D. Heather, P. Bu ingham, J. R. Healy, J. M. Gibbs, R. J. S. Wise, Y. Hatazawa, S. Hero R. P. Beany, D. J. Brooks, T. Spinks, C. Rhodes, R. S. J. Frackowiak, Jones, Cerebral blood flow, blood volume and oxygen utilizati normal values and effect of age. *Brain* **113**, 27–47 (1990).
33. J. B. Bassingthwaighte, I. S.J Chan, C. Y. Wang, Computationa efficient algorithms for convection-permeation-diffusion models blood-tissue exchange. *Ann. Biomed. Eng.* **20**, 687–725 (1992).